

# Final state interaction effects in $\mu$ -capture induced two-body decay of ${}^3\text{He}$ .

R.Skibiński\*, J.Golak\*, H.Wiśniewski<sup>\*,†</sup>, W.Glöckle<sup>†</sup>.

*\* Institute of Physics, Jagiellonian University, PL- 30059 Cracow, Poland*

*† Institut für theoretische Physik II, Ruhr-Universität Bochum, D-44780 Bochum, Germany*

(November 11, 2017)

## Abstract

The  $\mu$ -capture process on  ${}^3\text{He}$  leading to a neutron, a deuteron and a  $\mu$ -neutrino in the final state is studied. Three-nucleon Faddeev wave functions for the initial  ${}^3\text{He}$  bound and the final neutron-deuteron scattering states are calculated using the BonnB and Paris nucleon-nucleon potentials. The nuclear weak current operator is restricted to impulse approximation. Large effects on the decay rates of the final state interaction are found. The comparison to recent experimental data shows that the inclusion of final state interactions drastically improves the description of the data.

PACS numbers:

## I. INTRODUCTION.

Recently considerable progress has been achieved in the calculations of three nucleon (3N) continuum states. It is now possible to generate exact 3N bound [1] and scattering [2] states for any realistic nucleon - nucleon interaction even with inclusion of a three-nucleon force (3NF). This opens now the possibility to study the interaction of electromagnetic and/or weak probes with the 3N systems ( $^3\text{He}$  or  $^3\text{H}$  nuclei) without introducing into the analysis the uncertainties due to inadequate approximate 3N states. Only using such exact states nuclear dynamics can be tested with such probes and important information can be gained on the corresponding hadronic current operators.

Elastic and inelastic electron scattering on  $^3\text{He}$  ( $^3\text{H}$ ) as well as photodisintegration of  $^3\text{He}$  or  $\text{pd}$  capture are prominent examples of such processes and have been studied since many years with the hope to get insights into 3N bound state wave functions and into the hadronic current operator. As was shown in a series of recent papers on electromagnetic processes [3] [4] [5] a very important and unavoidable ingredient for their analysis is the exact treatment of the interaction among the three nucleons in the continuum states. It is also important, that the three-nucleon wave functions should be based on realistic nuclear forces. In this paper we would like to study the importance of final state interactions (FSI) between the nucleons in muon capture on  $^3\text{He}$ .

There are three final channels following the capture of a negative muon on  $^3\text{He}$ :

$$\begin{aligned}\mu^- + ^3\text{He} &\rightarrow ^3\text{H} + \nu_\mu, \\ \mu^- + ^3\text{He} &\rightarrow \text{d} + \text{n} + \nu_\mu, \\ \mu^- + ^3\text{He} &\rightarrow \text{p} + \text{n} + \text{n} + \nu_\mu.\end{aligned}\tag{1}$$

The capture rate for the  $^3\text{H} \nu_\mu$  channel has been extensively studied using the elementary particle method and the impulse approximation [6] [7]. When removing the nuclear uncertainties by using accurate three-body bound wave functions, this reaction offers the possibility to extract the induced pseudoscalar coupling constant with nearly the same precision as from the capture process by a free proton [7].

The old calculations of the total decay rates for the  $\text{dn}\nu_\mu$  (two-body breakup of  $^3\text{He}$ ) and  $\text{pnn}\nu_\mu$  (three-body breakup of  $^3\text{He}$ ) channels performed in [6] using the impulse approximation and 3N bound and scattering states generated within the Amado model with separable  $^1\text{S}_0$  and  $^3\text{S}_1$  two-nucleon interactions showed that scattering effects are large. The resulting total rates were in agreement with some of the limited and rather inaccurate experimental results while disagreed with others [6].

Recently the first measurement of energy spectra for deuteron and proton leaving  $^3\text{He}$  after nuclear muon capture leading to two-body and three-body breakup, respectively, has been reported [8] [9]. The partial capture rates were compared in [9] to simple plane wave impulse approximation calculations yielding fair agreement with the measured proton energy spectrum but underpredicting the measured rate of deuteron production by a large factor. It is the aim of the present paper to study if the inclusion of FSI by using an exact  $\text{n-d}$  scattering state can account for this discrepancy. In section II we describe our way to fully include FSI. In section III predictions for decay rates obtained with two realistic NN interactions: Bonn B [10] and Paris [11] are shown and compared to the experimental values. We conclude in section IV.

## II. THEORETICAL FORMALISM.

Fig.1. depicts the kinematics of the reaction. Our basis of the muon capture on  $^3\text{He}$  forms the more fundamental weak-interaction capture process on hydrogen:  $\mu^- + p \rightarrow n + \nu_\mu$ . The initial state

$$| i \rangle = | \Psi s_\mu \rangle | \Psi_{^3\text{He}} m P \rangle$$

is composed of the atomic K-shell muon wave function  $| \Psi s_\mu \rangle$  with spin projection  $s_\mu$  and the  $^3\text{He}$  state  $| \Psi_{^3\text{He}} m P \rangle$  with spin projection  $m$  and four momentum  $P$ . We choose the lab system with  $\vec{P} = 0$ . The transition leads to the final state

$$| f \rangle = | \nu_\mu s_\nu \rangle | \Psi^{(-)} P' \rangle .$$

where  $\nu_\mu$  is the four momentum of the neutrino and  $s_\nu$  its spin projection. The state  $| \Psi^{(-)} P' \rangle$  is the interacting neutron-deuteron state with overall four momentum  $P'$ .

The corresponding S-matrix element  $S_{fi}$  is given in first order perturbation theory and assuming the Fermi form for the interaction Lagrangian by

$$\begin{aligned} S_{fi} &= i \int d^4x \langle f | \mathcal{L}(x) | i \rangle = \\ &= i(2\pi)^4 \delta(P_f - P_i) \frac{G}{\sqrt{2}} * \\ &* \langle \Psi^{(-)} P' | I^\lambda(0) | \Psi_{^3\text{He}} m P \rangle * \langle \nu s_\nu | L_\lambda^\dagger(0) | \Psi s_\mu \rangle \\ &\equiv i(2\pi)^4 \delta(P_f - P_i) \frac{G}{\sqrt{2}} L_\lambda I^\lambda . \end{aligned} \quad (2)$$

The leptonic matrix element  $L_\lambda$  is known and is expressed in terms of the corresponding Dirac spinors for the neutrino  $u(\vec{\nu}, s_\nu)$  and the muon  $u(\vec{\mu}, s_\mu)$  by

$$L_\lambda = \frac{1}{(2\pi)^3} \bar{u}(\vec{\nu}, s_\nu) \gamma_\lambda (1 - \gamma_5) u(\vec{\mu}, s_\mu) . \quad (3)$$

In the nuclear matrix element neither the current operator  $I^\lambda(0)$  nor the nuclear wave functions are equally well under control. In the following we restrict ourselves to the impulse approximation (IA) and neglect the exchange current effects. The single nucleon current operator is parametrized in terms of weak-interaction formfactors  $g_i^{V,A}$  [12]

$$\begin{aligned} I^\lambda(0) &= \frac{1}{(2\pi)^3} \sum_{s,s'} \sum_{\tau,\tau'} \int d\vec{p} d\vec{p}' a^\dagger(\vec{p}, s, \tau) \bar{u}(\vec{p}, s) * \\ &* \{ (g_1^V - 2mg_2^V) \gamma^\lambda + g_2^V (p + p')^\lambda + g_1^A \gamma^\lambda \gamma^5 + g_2^A k^\lambda \gamma^5 \} * \\ &* \tau_- u(\vec{p}', s') a(\vec{p}', s', \tau') , \end{aligned} \quad (4)$$

where  $a, a^\dagger$  are standard nucleon creation and annihilation operators,  $\tau_-$  is the isospin lowering operator and  $k \equiv p' - p$ . For the nucleon weak formfactors we use the standard values [13]

$$\begin{aligned}
g_1^V(k^2) &= \frac{1}{(1 + \frac{k^2}{0.71 [GeV]^2})^2} , \\
g_1^A(k^2) &= \frac{-1.262}{(1 + \frac{k^2}{1.19 [GeV]^2})^2} , \\
2mg_2^V(k^2) &= \frac{-3.7}{(1 + \frac{k^2}{0.71 [GeV]^2})^2} , \\
g_2^A(k^2) &= \frac{-2mg_1^A(k^2)}{k^2 + m_\pi^2} ,
\end{aligned} \tag{5}$$

with  $m_\pi = 138.13$  MeV.

Nuclear wave functions are generated by the nonrelativistic Schrödinger equation with realistic nuclear forces. Therefore to be consistent, the nuclear-current should also be chosen nonrelativistically. After a nonrelativistic reduction of (4) and introducing standard Jacobi momenta  $\vec{p}, \vec{q}$  one gets for  $I^\lambda$  defined in Eq.(2)

$$I^\lambda = \langle \Psi^{(-)} | i^\lambda | \Psi_{^3\text{He}} m \rangle , \tag{6}$$

where the momentum space matrix elements of  $i^\lambda$  are

$$\begin{aligned}
\langle \vec{p}\vec{q} | i^\lambda(\vec{Q}) | \vec{p}'\vec{q}' \rangle &= \delta(\vec{p}' - \vec{p})\delta(\vec{q}' - (\vec{q} - \frac{2}{3}\vec{Q}))I^\lambda(\vec{q}, \vec{Q}) , \\
I^0(\vec{q}, \vec{Q}) &= \frac{3}{(2\pi)^3} \{ g_1^V + g_1^A (\frac{\vec{\sigma}\vec{\pi}}{m} - \frac{\vec{\sigma}\vec{\nu}}{2m}) \} , \\
\vec{I}(\vec{q}, \vec{Q}) &= \frac{3}{(2\pi)^3} \{ g_1^V (\frac{\vec{\pi}}{m} - \frac{\vec{\nu}}{2m}) - \frac{\nu}{2m} (g_1^V + g_2^V 2m) i(\vec{\sigma} \times \hat{\nu}) + \\
&\quad + g_1^A \vec{\sigma} - g_2^A \frac{1}{2m} m_\mu \hat{\nu} (\vec{\sigma}\vec{\nu}) \} ,
\end{aligned} \tag{7}$$

with  $\vec{\pi} \equiv \frac{2}{3}\vec{\nu} + \vec{q}$ ;  $\vec{\nu} = -\vec{Q}$ . The treatment of the final state follows [3] [4]. For the convenience of the reader we repeat the most important steps.

The final scattering state  $|\Psi^{(-)}\rangle = |\Psi_{nd}^{(-)}\rangle$  is decomposed into Faddeev components  $|F_1\rangle$

$$|\Psi_{nd}^{(-)}\rangle \equiv \frac{1}{\sqrt{3}}(1 + P) |F_1\rangle , \tag{8}$$

where  $P$  is a sum of cyclical and anticyclical permutations of three nucleons. The Faddeev component obeys the equation

$$|F_1\rangle = |\Phi_{nd}\rangle + G_0^{(-)} t_1^{(-)} P |F_1\rangle , \tag{9}$$

and the state  $|\Phi_{nd}\rangle$  describes the free relative motion of the final nucleon and the deuteron. Inserting (8) and (9) into (6) yields

$$I^\mu = I_{PWIAS}^\mu + I_{rescatt}^\mu , \tag{10}$$

where  $I_{PWIAS}^\mu$  (symmetrized plane wave impulse approximation) corresponds to the case that in Eq.(6)  $\langle \Psi^{(-)} |$  is replaced by  $\frac{1}{\sqrt{3}} \langle \Phi_{nd} | (1 + P)$  and therefore no interactions between the outgoing nucleon and the deuteron are present. For the  $I_{rescatt}^\mu$  term, which contains all rescattering,  $\langle \Psi^{(-)} |$  is replaced by  $\frac{1}{\sqrt{3}} \langle F_1 | P t_1 G_0 (1 + P)$ . The rescattering term can be written as [3] [4]

$$I_{rescatt}^\mu \equiv \frac{1}{\sqrt{3}} \langle \Phi_{nd} | P | U^\mu \rangle, \quad (11)$$

with

$$| U^\mu \rangle = t_1 G_0 (1 + P) i^\mu(\vec{Q}) | \Psi_{3\text{He}} \rangle + t_1 G_0 P | U^\mu \rangle. \quad (12)$$

This integral equation has the same integral kernel which one also finds in the 3N continuum [2] and the same numerical methods can be used to solve it for any NN interaction. We solve Eq.(12) in a partial wave decomposition and in momentum space. For details we refer to [2] [14] [15] [16]. The decay rate follows from  $S_{fi}$  in a standard way [17] and for the capture process with an unpolarized initial state and without polarization of the outgoing particles, it is given by

$$\begin{aligned} d\Gamma &= (2\pi)^2 \frac{1}{2} \frac{1}{2} \frac{(2m'\alpha)^3}{\pi} \int d\vec{\nu} d\vec{p}_d d\vec{p}_n \delta(P - \nu - p_d - p_n) (2\pi)^8 \frac{G^2}{2} \sum_{\substack{m_{3\text{He}} \\ m_{s\mu}}} \sum_{\substack{m_{s\nu} \\ m_n, m_d}} |L_\lambda I^\lambda|^2 \quad (13) \\ &= 8\pi^2 (2\pi)^2 \frac{1}{2} \frac{1}{2} \frac{(2m'\alpha)^3}{\pi} \int E_\nu m_n m_d dE_\nu dE_d (2\pi)^8 \frac{G^2}{2} \sum_{\substack{m_{3\text{He}} \\ m_{s\mu}}} \sum_{\substack{m_{s\nu} \\ m_d}} |L_\lambda I^\lambda|^2, \end{aligned}$$

with  $P = (m_\mu + m_{3\text{He}}, \vec{0})$  in the lab. system and  $m' = \frac{m_\mu m_{3\text{He}}}{m_\mu + m_{3\text{He}}}$ . The factors in (13) come from averaging over the spin of the initial particles,  $(\frac{1}{2}\frac{1}{2})$ , from the states normalizations,  $((2\pi)^2(2\pi)^8)$ , and from the muon wave function (which is taken as an atomic K-shell wave function),  $(\frac{(2m'\alpha)^3}{\pi})$ , with  $\alpha = \frac{1}{137.036}$ .

### III. RESULTS AND COMPARISON WITH EXPERIMENTAL DATA.

To calculate the decay rates one has to evaluate the nuclear matrix elements  $I^\lambda$ . The initial 3N bound state of  $^3\text{He}$  is always based on a 34 channel Faddeev calculation. In treating the 3N continuum we included all 3N partial waves with total NN angular momenta up to  $j_{max} = 2$ . In order to check the convergence of the results also calculations restricted to 3N states with  $^1S_0 + ^3S_1 - ^3D_1$  NN force components only and with  $j_{max} = 1$  have been performed. As NN force we use the Bonn B [10] and Paris [11] potentials. Let us first consider the case of a kinematically complete situation in the outgoing n-d channel. Since the outgoing channel contains 3 particles and the decay originates from an initial state of zero momentum one needs only 2 kinematical parameters to completely define the momenta of the outgoing particles. For these 2 parameters the neutrino and deuteron energies  $E_\nu$  and  $E_d$  can be taken. The kinematically allowed range of neutrino energies is  $E_\nu \in [0, E_\nu^{max}]$  with

$$E_\nu^{max} = \frac{(m_\mu + m_{3\text{He}})^2 - (3m_n - |E_D|)^2}{2(m_\mu + m_{3\text{He}})}. \quad (14)$$

For each neutrino energy there is a range of allowed deuteron energies as shown in Fig.2. Each deuteron energy corresponds to a unique angle between neutrino and deuteron momenta. In Fig.3 we show decay rates  $\frac{d^2\Gamma}{dE_d dE_\nu}$  for two values of the deuteron energy. There is a drastic increase in decay rates by a factor of  $\approx 200$ , when the interactions between the neutron and the deuteron in the final state are included. The increase is practically independent from the deuteron and neutrino energies. Fig.4 shows that the results obtained restricting to  $j_{max} = 2$  NN force components might be not yet fully converged. Nevertheless as is clear from Fig.5 they are sufficient to analyse the existing data. The drastic effects of FSI show that any analysis of the experimental data should be based on realistic continuum wave functions.

Up to now only one data set for the  $\mu$ -capture on  $^3\text{He}$  leading to the  $n + d + \nu_\mu$  outgoing channel exists [8] [9]. In order to compare our results to those data one has to numerically integrate the decay rate at every deuteron energy over the unobserved neutrino energy. This leads to the results presented in Fig.5. It is clearly seen that while the PWIAS predictions drastically underestimate the data, the inclusion of FSI leads to a rather good agreement, which is fairly independent from the NN interaction used. Also the convergence in  $j_{max}$  is similar to the kinematically complete cases as can be seen in Fig.6.

#### IV. SUMMARY AND CONCLUSIONS.

We calculated the decay rates for muon capture on  $^3\text{He}$  leading to the  $n+d+\nu_\mu$  channel. Realistic NN forces have been used (Bonn B and Paris potentials) and both the 3N bound state and the 3N continuum scattering wave functions were evaluated consistently solving the corresponding Faddeev equations. We used the most simple nonrelativistic single nucleon weak-current operator parametrized by the standard nucleon weak formfactors. Both in the kinematically complete and the uncomplete situations the predictions of the plane-wave impulse approximation for the final neutron-deuteron state drastically differ by a factor of about  $\sim 200$  from the full result including final state interaction. The comparison to the only existing uncomplete data for this process reveals, that a good description of the data only results when the FSI is taken into account. The total failure of PWIAS in describing those data shows that any future analysis of this process should be performed with bound and scattering states generated consistently from a realistic 3N Hamiltonian. From the theoretical point of view mesonic exchange currents should also be added in future analysis.

#### A. Acknowledgements.

This work was supported by the Polish Committee for Scientific Research under Grant No. 2P03B03914. The numerical calculations were performed on the Cray T90 and T3E of the Höchstleistungsrechenzentrum in Jülich, Germany and on the Convex 3840 of the ACK-Cyfronet, Cracow, Poland under Grant No. KBN/C3840/UJ/020/1994.

## REFERENCES

- [1] A.Nogga, D.Hüber, H.Kamada, W.Glöckle, Phys.Lett. **B409**, 19 (1997) and references therein.
- [2] W.Glöckle, H.Wiła, D.Hüber, H.Kamada, J.Golak, Phys.Rep **274**, 107 (1996).
- [3] S.Ishikawa, H.Kamada, W.Glöckle, J.Golak, H.Wiła, Il Nuovo Cimento **107A**, 305 (1994).
- [4] J.Golak, H.Kamada, H.Wiła, W.Glöckle, S.Ishikawa, Phys.Rev. **C51**, 1638 (1995).
- [5] W.Glöckle, J.Golak, H.Kamada, H.Wiła, S.Ishikawa, D.Hüber, in Procced. of the Workshop on Electronuclear Physics with Internal Targets and the BLAST Detectors, MIT, May 1998.
- [6] A.C.Phillips, F.Roig, J.Ros, Nucl.Phys. **A237**, 493 (1975).
- [7] J.S.Congleton, H.W.Fearing, Nucl.Phys. **A552**, 534 (1993).
- [8] W.J.Cummings, G.E.Dodge, S.S.Hanna, B.H.King, S.E.Kuhn, Y.M.Shin, R.Helmer, R.B.Schubank, N.R.Stevenson, U.Wienands, Y.K.Lee, G.R.Mason, B.E.King, K.S.Chung, J.M.Lee, D.R.Rosenzweig, Phys.Rev.Lett. **68**, 293 (1992).
- [9] S.E.Kuhn, W.J.Cummings, R.Helmer, R.B.Schubank, G.E.Dodge, S.S.Hanna, B.H.King, Y.M.Shin, J.G.Congleton, N.R.Stevenson, U.Wienands, Y.K.Lee, G.R.Mason, B.E.King, K.S.Chung, J.M.Lee, D.R.Rosenzweig, Phys.Rev. **C50**, 1771 (1994).
- [10] R.Machleidt, Adv.Nucl.Phys. **19**, 189 (1989);  
R.Machleidt, K.Holinde, Ch.Elster, Phys Rep. **149**, 1 (1987).
- [11] M.Lacombe, B.Loiseau, J.M.Richard, R.Vinh Mau, J.Cote, P.Pires, R. de Turreill Phys.Rev. **C21**, 861 (1980).
- [12] D.Bailin, Weak Interactions, Adam Hilger LTD, Bristol 1982.
- [13] N.Tatara, Y.Kohyama, K.Kubodera, Phys.Rev. **C42**, 1694 (1990).
- [14] W.Glöckle, The Quantum Mechanical Few-Body Problem, Springer Verlag, Berlin, 1983.
- [15] W.Glöckle, Lecture Notes in Physics **273**, 3 (1987).
- [16] H.Wiła, W.Glöckle, Th.Cornelius, Few-Body Systems **3**, 123 (1988).
- [17] A.D.Matrin, T.D.Spearman, Elementary Particle Theory, North-Holland Publishing Company, 1970.

## Figure Captions

Fig.1 Kinematics for the  $\mu^- + {}^3\text{He} \rightarrow \text{n} + \text{d} + \nu_\mu$  reaction.

Fig.2 Kinematically allowed neutrino and deuteron energies.

Fig.3 The decay rate  $\frac{d^2\Gamma}{dE_d dE_\nu}$  at two values of the deuteron energy  $E_d = 18$  MeV and  $E_d = 29$  MeV. The dashed and dotted lines are the PWIAS predictions for the Bonn B and Paris potentials, respectively. The solid and dashed-dotted lines are the Bonn B and Paris potential predictions when in the final state all NN force components up to  $j_{\text{max}} = 1$  are included.

Fig.4 The convergence in  $j_{\text{max}}$  of the decay rate  $\frac{d^2\Gamma}{dE_d dE_\nu}$  at two deuteron energies as in Fig.3. The dotted, dashed and solid lines correspond to  ${}^1S_0 + {}^3S_1 - {}^3D_1$ ,  $j_{\text{max}} = 1$  and  $j_{\text{max}} = 2$  Bonn B calculations, respectively.

Fig.5 The decay rate  $\frac{d\Gamma}{dE_d}$  for the case when neutrino is not observed. For the description of lines see Fig.3. The squares are experimental points from [8] [9].

Fig.6 The convergence in  $j_{\text{max}}$  of the decay rate  $\frac{d\Gamma}{dE_d}$ . For the description of lines see Fig.4. The squares are experimental points as in Fig.5.



# FIGURES

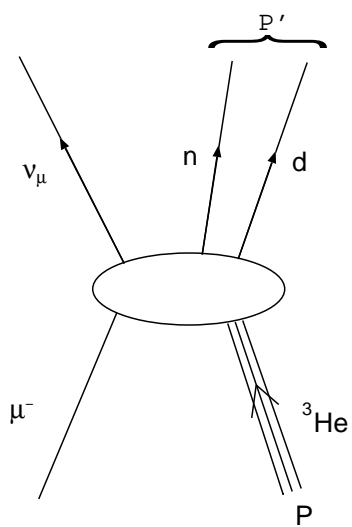


FIG. 1. Kinematics for the  $\mu^- + {}^3\text{He} \rightarrow n + d + \nu_\mu$  reaction.

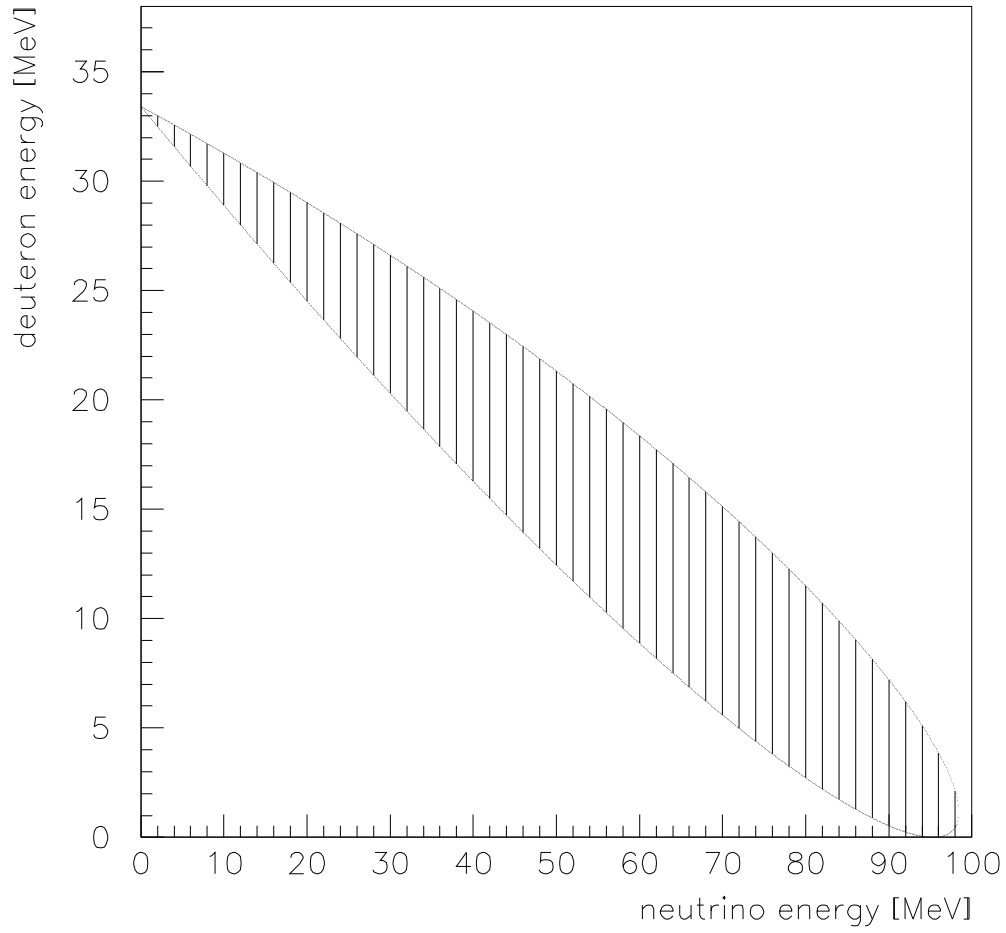


FIG. 2. Kinematically allowed neutrino and deuteron energies.

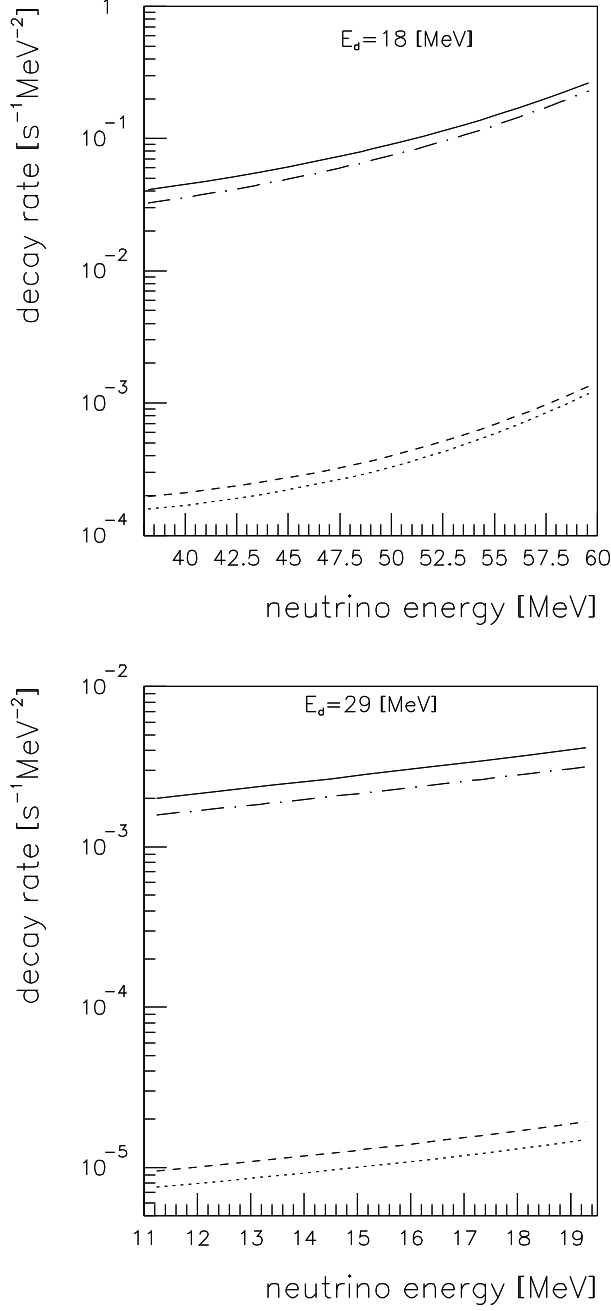


FIG. 3. The decay rate  $\frac{d^2\Gamma}{dE_d dE_\nu}$  at two values of the deuteron energy  $E_d = 18$  MeV and  $E_d = 29$  MeV. The dashed and dotted lines are the PWIAS predictions for the Bonn B and Paris potentials, respectively. The solid and dashed-dotted lines are the Bonn B and Paris potential predictions when in the final state all NN force components up to  $j_{\text{max}} = 1$  are included.

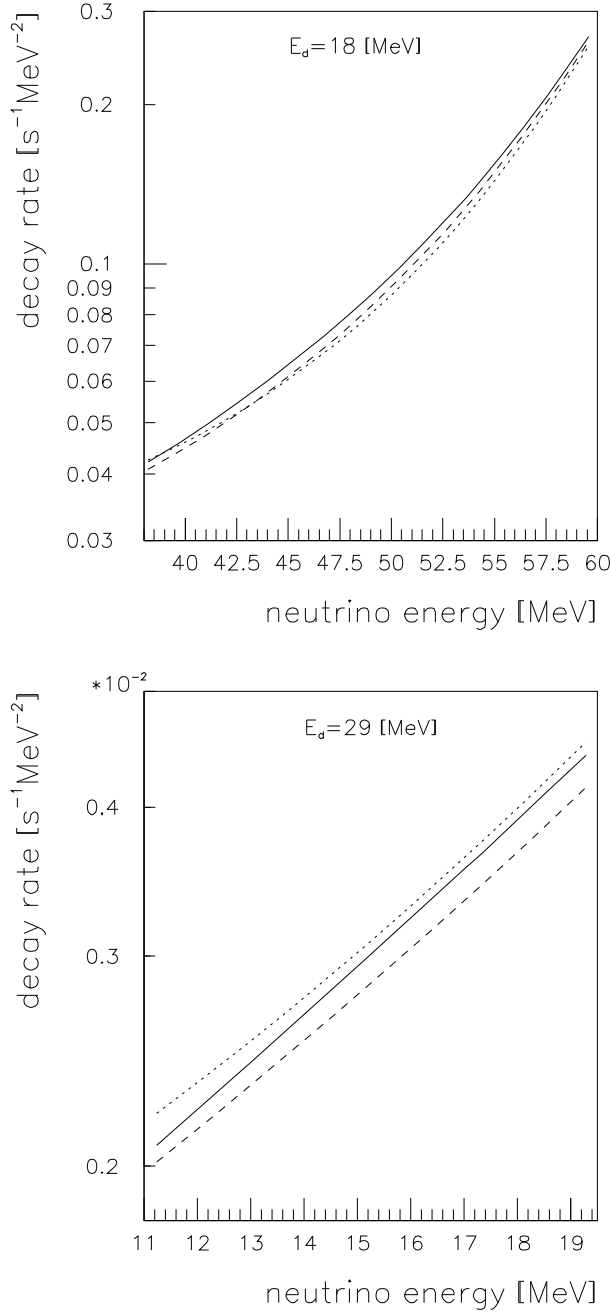


FIG. 4. The convergence in  $j_{\text{max}}$  of the decay rate  $\frac{d^2\Gamma}{dE_d dE_\nu}$  at two deuteron energies as in Fig.3. The dotted, dashed and solid lines correspond to  $^1S_0 + ^3S_1 - ^3D_1$ ,  $j_{\text{max}} = 1$  and  $j_{\text{max}} = 2$  Bonn B calculations, respectively.

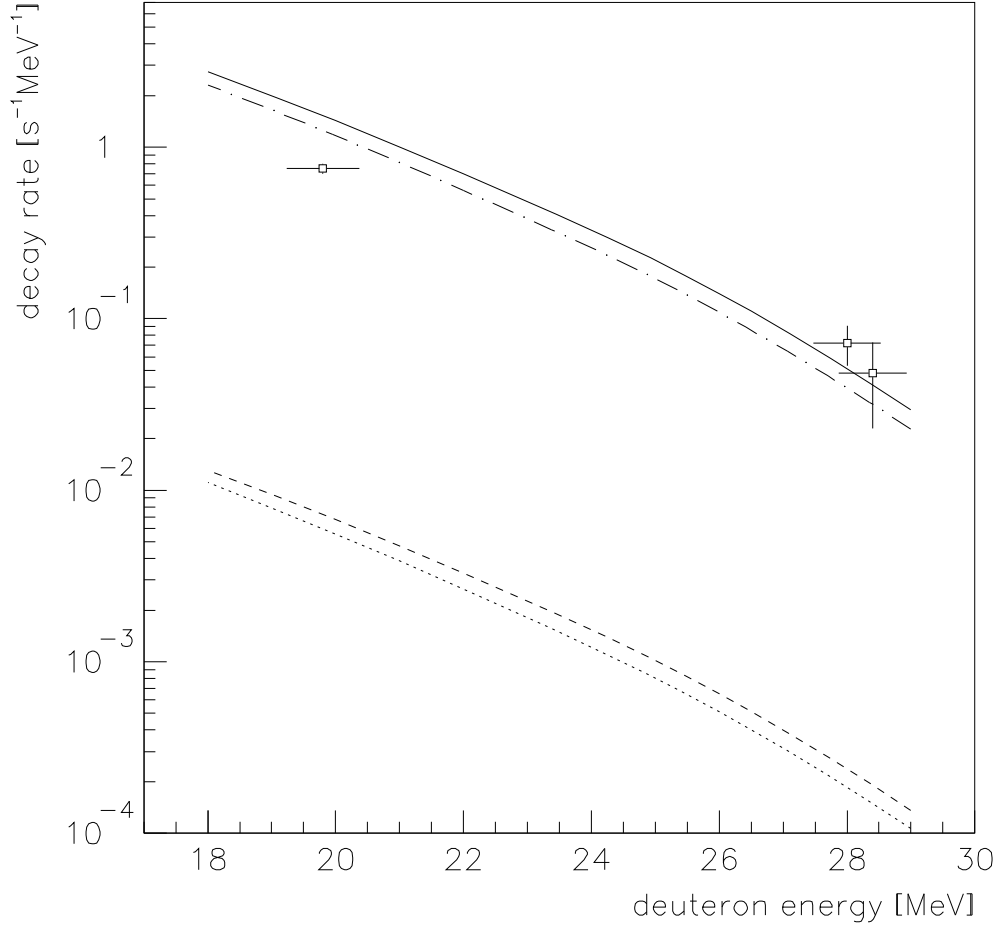


FIG. 5. The decay rate  $\frac{d\Gamma}{dE_d}$  for the case when neutrino is not observed. For the description of lines see Fig.3. The squares are experimental points from (8) (9).

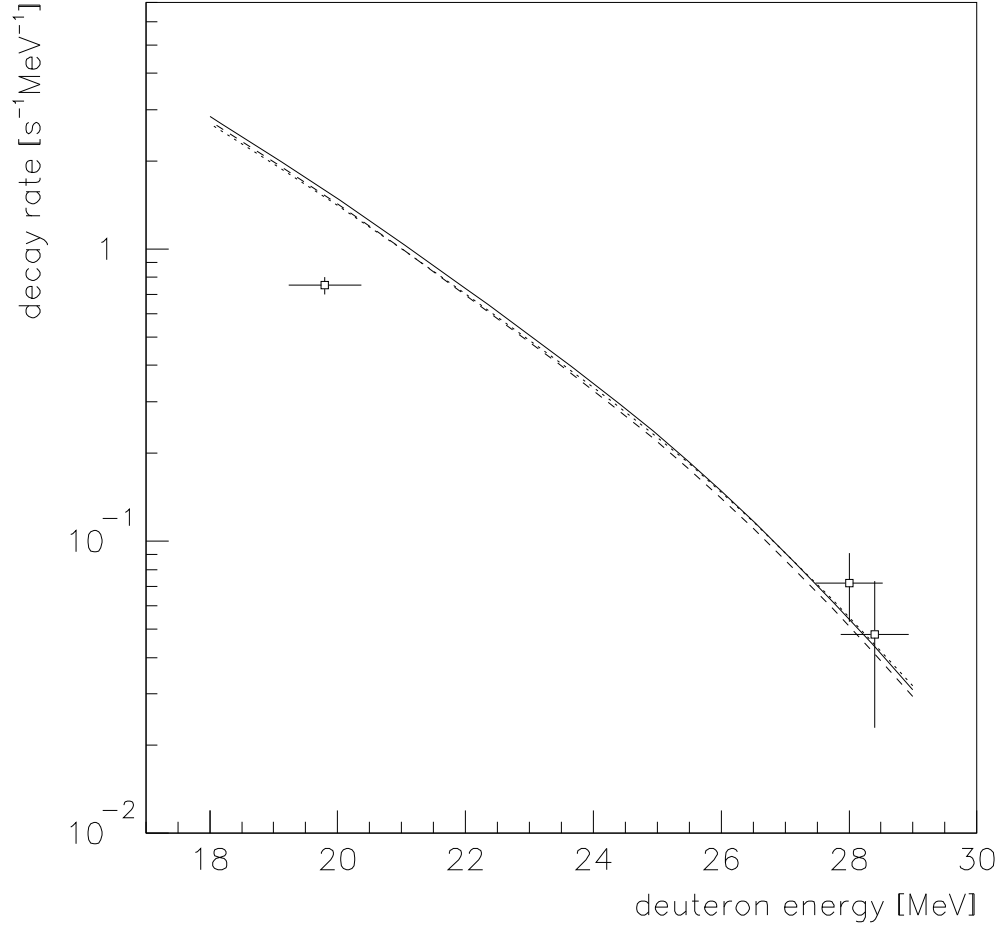


FIG. 6. The convergence in  $j_{\max}$  of the decay rate  $\frac{d\Gamma}{dE_d}$ . For the description of lines see Fig.4. The squares are experimental points as in Fig.5.